Nuclear “ bubble” structure in 34Si

Grasso, M.; Gaudefroy, L.; Khan, E.; Nikšić, Tamara; Piekarewicz, J.; Sorlin, O.; Giai, N. Van; Vretenar, Dario

Nuclear "bubble" structure in ^{34}Si

M. Grasso,[1] L. Gaudefroy,[2] E. Khan,[1] T. Nikšić,[3] J. Piekarewicz,[4] O. Sorlin,[5] N. Van Giai,[1] and D. Vretenar[3]

[1]*Institut de Physique Nucléaire, Université Paris-Sud, IN2P3-CNRS, F-91406 Orsay Cedex, France*

[2]*CEA, DAM, DIF, F-91297 Arpajon, France*

[3]*Physics Department, Faculty of Science, Zagreb University, HR-10000 Zagreb, Croatia*

[4]*Florida State University, Tallahassee, Florida 32306, USA*

[5]*Grand Accélerateur National d'Ions Lourds (GANIL), CEA/DSM-CNRS-IN2P3, Boulevard Henri Becquerel, Boîte Postale 55027, F-14076 Caen Cedex 5, France*

(Received 22 September 2008; revised manuscript received 10 February 2009; published 26 March 2009)

Bubble nuclei are characterized by a depletion of their central density. Their existence is examined within three different theoretical frameworks: the shell model and nonrelativistic and relativistic microscopic mean-field approaches. We analyze ^{34}Si and ^{22}O as possible candidates for proton and neutron bubble nuclei, respectively. In the case of ^{22}O, we observe a significant model dependence, thereby calling into question the bubble structure of ^{22}O. In contrast, an overall agreement among the models is obtained for ^{34}Si. Indeed, all models predict a central proton density depletion of about 40% and a central charge density depletion of 25%–30%. This result provides strong evidence in favor of a proton bubble in ^{34}Si.

DOI: 10.1103/PhysRevC.79.034318 PACS number(s): 21.10.Ft, 21.60.−n, 25.30.Bf, 27.30.+t

I. INTRODUCTION

The "bubble" structure of atomic nuclei is characterized by a depleted central density. Although it is somewhat unexpected that a "hole" can be made in a nuclear system where nuclear forces generate a saturation density ($\rho_0 \sim 0.16$ fm^{-3}), this phenomenon has been discussed for many decades. Indeed, the possibility of bubble nuclei started with the pioneering work of Wilson in the 1940s [1], who studied the low-energy excitations of a thin spherical shell, up to the first microscopic calculations of Campi and Sprung in the 1970s [2]. More recently, bubbles have been discussed in superheavy and hyperheavy nuclei [3,4]. The promise of producing more exotic nuclei with the new generation of RIB facilities has revived interest in this subject.

Owing to the absence of a centrifugal barrier, s orbitals have radial distributions peaked in the interior of the nucleus, with their corresponding wave function extending further into the surface depending on the number of nodes. In contrast, orbitals with nonzero angular momenta are suppressed in the nuclear interior and do not contribute to the central density. Therefore, any vacancy of s orbitals is expected to produce a depletion of the central density. By using electron scattering from ^{206}Pb and ^{205}Tl up to large momentum transfers, the radial distribution of the 3s proton orbital was experimentally mapped and shown to closely resemble the one predicted by an independent particle model. The agreement extends from the center of the ^{206}Pb nucleus all the way to the surface and reproduces accurately the nodal structure of the wave function [5,6]. Differences in the charge density between ^{206}Pb and ^{205}Tl revealed that about 80% of the proton removal strength came from the 3s state, thereby leading to a depletion of the proton density in the nuclear interior. Specifically, the depletion fraction, defined as

$$F \equiv \frac{\rho_{\max} - \rho_c}{\rho_{\max}}, \tag{1}$$

amounts to $F = 11(2)\%$. In this equation ρ_c and $\rho_{\max}$ represent the values of the central and maximum charge density in ^{205}Tl, respectively. Yet the small energy difference between the $3s_{1/2}$ and the $2d_{3/2}$ proton orbitals plus the coupling of the $3s_{1/2}$ proton to collective excitations in ^{206}Pb yield a proton hole strength in ^{205}Tl that is shared among the $3s_{1/2}$ and $2d_{3/2}$ orbitals, with the former carrying about 70% of the strength and the latter the remaining 30%. Consequently, the central depletion in ^{205}Tl relative to ^{206}Pb is not as large as if the full hole strength would have been carried by the 3s orbital. Using similar arguments, one can conclude that the depletion at the center of ^{204}Hg is not expected to be very large, as the two-proton hole strength will be again shared among the $3s_{1/2}$ and $2d_{3/2}$ orbitals. Therefore, the search for the best bubble candidates should be oriented toward nuclei with an s orbital well separated from its nearby single-particle states and where correlations are weak. This latter feature arises mainly for nuclei located at major shell closures.

Recently, the formation of a proton bubble resulting from the depletion of the $2s_{1/2}$ orbital was investigated in ^{46}Ar [7,8] and in the very neutron rich Ar isotopes [8]. In ^{46}Ar the proton $2s_{1/2}$ and $1d_{3/2}$ orbitals are almost degenerate: As in the case of ^{206}Pb, pairing correlations will lead to a significant occupancy of the $2s_{1/2}$ orbital [9], thus weakening the bubble effect. This weakening will continue to hold for any $N = 28$ isotone between $Z = 20$ and $Z = 14$ as long as the $2s_{1/2}$ and $1d_{3/2}$ orbitals remain degenerate, as shown for instance in Fig. 3 of Ref. [10]. For very neutron rich Ar isotopes, such as ^{68}Ar, the $s_{1/2}$ proton orbital is predicted to move significantly above the $d_{3/2}$ state, hindering the role of pairing correlations [8,11]. Unfortunately, the production of this exotic nucleus is far beyond the present and near-future capabilities of RIB facilities.

A more suitable region of the chart of the nuclides to search for a proton bubble is that of the $N = 20$ isotones. Between $Z = 20$ and $Z = 16$ the $s_{1/2}$ orbital is located about 6.5 MeV above the $d_{5/2}$ orbital and about 2.5 MeV below the $d_{3/2}$ orbital,

thereby forming two subshell closures at $Z = 14$ and $Z = 16$, respectively [12]. In addition, the $N = 20$ shell closure is rigid enough to hinder significant coupling to collective states. If one assumes a sequential filling of proton orbitals, the $2s_{1/2}$ orbital should be completely empty in ^{34}Si but fully filled in ^{36}S. This may lead to an important change in the proton density distribution between ^{36}S and ^{34}Si, making ^{34}Si an excellent candidate for a bubble nucleus. Concomitantly, both Skyrme and Gogny Hartree-Fock-Bogoliubov models predict a spherical shape for ^{34}Si [13,14]. Other possible candidates in the Si-isotopic chain, such as ^{28}Si and ^{42}Si, are not optimal as they are deformed [15,16]. For these nuclei several correlations hinder the development of a bubble. The mirror system of (^{36}S, ^{34}Si), (^{36}Ca, ^{34}Ca), could not be studied at present because the ^{34}Ca nucleus has not been observed so far.

A neutron bubble may be found in the oxygen chain, where large $N = 14$ (between $d_{5/2}$ and $s_{1/2}$) and $N = 16$ (between $s_{1/2}$ and $d_{3/2}$) subshell gaps of about 4.2 MeV [17,18] and 4 MeV [19], respectively, have been determined. Combined with the large proton gap at $Z = 8$, ^{22}O [17,20,21] and ^{24}O [18,19,22] therefore behave as doubly magic nuclei. In this case the change in the occupancy of the $2s_{1/2}$ neutron orbital will occur between ^{22}O and ^{24}O, making ^{22}O a good candidate for a neutron bubble nucleus.

The present article aims at determining whether ^{34}Si and ^{22}O could be considered as good proton and neutron bubble nuclei, respectively. Various theoretical approaches will be employed to test the robustness of the results. In Sec. II these nuclei are analyzed in terms of shell-model calculations and the occupancies of the proton and neutron orbitals are determined. In Sec. III we first address the role of pairing correlations in mean-field approaches and then show results on microscopic nucleon density profiles obtained from (i) non-relativistic Hartree-Fock (HF) and Hartree-Fock-Bogoliubov (HFB) and (ii) relativistic mean-field (RMF) and relativistic Hartree-Bogoliubov (RHB) microscopic calculations. Comparisons to experimental data will be made whenever possible. Conclusions are drawn in Sec. IV.

II. SHELL-MODEL PREDICTIONS

The occurrence of bubbles in nuclei, as previously defined, is directly linked to the occupancy of $s_{1/2}$ orbitals. For both bubble candidates under study in this article, ^{22}O and ^{34}Si, experimental values for the occupancies are not yet available. Thus, we rely hereafter on shell-model (SM) calculations to estimate the occupation numbers of interest. Calculations have been performed with the ANTOINE code [23,24] using the USD interaction [25]. The full sd valence space was considered for protons and neutrons to study the ground-state configuration of the nuclei under consideration.

Special care should be taken concerning the contamination of the physical states of interest by spurious states originating from the center-of-mass (CM) translation. The internal structure of a nucleus with N nucleons is described by $3N - 3$ coordinates giving the relative positions of its constituents. The three remaining degrees of freedom describe the CM motion of the whole nucleus and give rise to spurious CM effects that modify the properties of the physical states such as binding energies and occupation numbers, as already shown by Dieperink and de Forest [26]. Following the work presented in Ref. [26], it is possible to obtain CM-corrected occupation numbers, referred to as S' in the following, from the occupation numbers S calculated within the SM framework. For the $2s_{1/2}$ and $1d_{3/2,5/2}$ orbits, the relation $S'_{sd} = \left(\frac{A}{A-1}\right)^2 S_{sd}$ holds, where A is the mass number of the considered nucleus. The corrected occupation numbers for $1p$ orbits are defined as $S'_{1p} = \frac{A}{A-1}(S_{1p} - \frac{2S_{sd}}{A-1})$ for the nuclei under consideration in this article. Finally, the sum rule on occupation numbers allows us to deduce the CM-corrected value for the deeply bound $1s_{1/2}$ orbit as

$$S'_{1s} = M - \sum_{\alpha \neq 1s} S'_{\alpha},$$

where M is either the neutron or the proton number of the considered nucleus.

The nucleon densities presented in the following have been evaluated by using the wave functions of a Woods-Saxon potential (without spin-orbit term), with parameters $V_0 = -50$ MeV, $a = 0.65$ fm, and $r_0 = 1.25$ fm [27], and the SM occupation numbers corrected for CM effects. One notices that not considering the spin-orbit interaction leads to the same radial dependence for wave functions of nucleons occupying orbits with the same principal quantum number (n) and orbital angular momentum (ℓ), but with different total angular momentum (J), as for the $1p_{3/2}$ and $1p_{1/2}$ orbitals.

A. Neutron bubble: ^{24}O and ^{22}O

The mean occupation numbers S and S' of neutron orbits deduced from SM calculations are reported in Table I. The difference of the neutron $2s_{1/2}$ occupancy between ^{24}O to ^{22}O amounts to 1.69, where a value of 2 was expected without nuclear correlations. The remaining neutron strength is mainly taken from the $\nu d_{5/2}$ and to a lesser extent from the $\nu d_{3/2}$ orbital. As a result of the depletion of the $1s_{1/2}$ and $1p$ inner shells, the S' occupation numbers for the $\nu 1d_{5/2}$ and $\nu 2s_{1/2}$ orbits in ^{24}O slightly exceed the standard value of $(2J + 1)$ (see Table I).

The neutron densities of ^{22,24}O shown in Fig. 1 include the CM correction just discussed. The effect of the removal of two neutrons between ^{24}O and ^{22}O is clearly visible from the comparison of their densities. The effect of the CM correction

TABLE I. Ground-state occupation numbers S of neutron orbits obtained in the present SM calculations for ^{24}O and ^{22}O. The corresponding values S', corrected for CM effects, are also reported.

Orbital	$S(^{24}\mathrm{O})$	$S'(^{24}\mathrm{O})$	$S(^{22}\mathrm{O})$	$S'(^{22}\mathrm{O})$
$\nu 1s_{1/2}$	2.00	1.75	2.00	1.73
$\nu 1p_{3/2}$	4.00	3.69	4.00	3.79
$\nu 1p_{1/2}$	2.00	1.85	2.00	1.90
$\nu 1d_{5/2}$	5.75	6.26	5.38	5.91
$\nu 2s_{1/2}$	1.89	2.06	0.34	0.37
$\nu 1d_{3/2}$	0.36	0.39	0.28	0.31

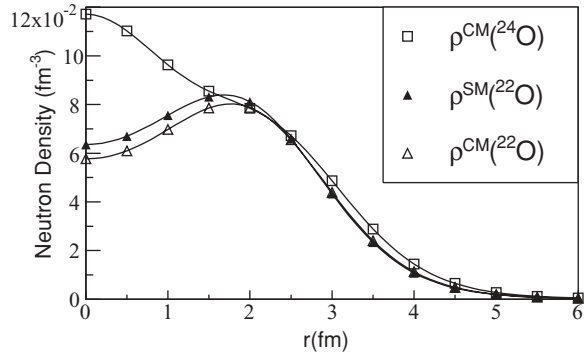

FIG. 1. Neutron densities of ^{24}O and ^{22}O (open squares and triangles, respectively) obtained using the occupation numbers corrected for CM motion and Woods-Saxon wave functions. The density of ^{22}O without CM correction is also shown (black triangles).

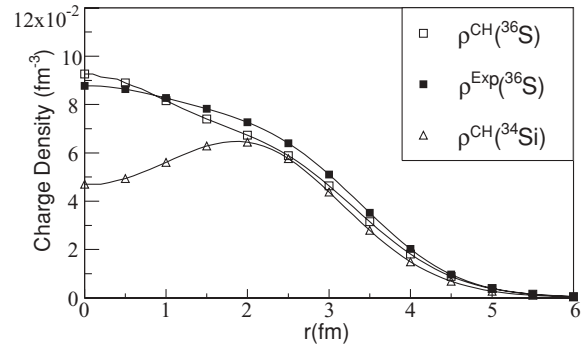

FIG. 2. Same as Fig. 1 but for charge densities in ^{36}S and ^{34}Si (see text).

is to slightly deepen the density profile at small radial distances ($r < 2$ fm). Indeed the depletion fraction in ^{22}O, as defined in Eq. (1), is found to be 28% for the CM-corrected density (open triangles on Fig. 1) and 24% for the uncorrected density (filled triangles).

In lighter oxygen isotopes this central depletion should not persist as the neutron $1d_{5/2}$ orbital, located at the surface of the nucleus, is depleted in concert with the $2s_{1/2}$. It follows that the relative difference of the density in the vicinity of the surface and at the interior of the nucleus is also reduced.

B. Proton bubble: ^{36}S and ^{34}Si

The mean occupation numbers of the proton $1d_{3/2}$ (0.31), $2s_{1/2}$ (1.63), and $1d_{5/2}$ (5.95) orbitals in ^{36}S have been obtained from the ^{36}S(d, ^{3}He)^{35}P experiment [28]. The small occupancy of the $1d_{3/2}$ state is due to correlations. The sum of the deduced spectroscopic factors from the proton pickup reaction from the whole sd states amounts to $\sum C^2S \approx 7.9$. Within the 20% uncertainties of the method, this is compatible with $\sum C^2S = 8$. The mean calculated occupation numbers S for the proton orbitals, as well as those corrected for CM motion, S', are reported in Table II. The agreement with the experimental values for ^{36}S is very good, lending confidence to the SM predictions for ^{34}Si. The mean occupation number in ^{34}Si, summed over the $1s$ and $2s$ orbits, is smaller than in ^{22}O. Moreover, a larger mean occupation number of the $d_{5/2}$ orbital is predicted in ^{34}Si as compared to ^{22}O. Both effects, that is, weaker (larger) occupancy at the center (surface), account for the depletion fraction in the proton density of ^{34}Si found to be $F = 44\%$ ($F = 41\%$) with (without) the CM corrections. The charge densities displayed on Fig. 2 for ^{34}Si and ^{36}S are obtained by including CM and proton finite-size corrections. The resulting value of F for ^{34}Si is $F = 28\%$. It has been shown in the previous section that the effect of the CM correction is to increase the bubble; this means that the proton finite-size correction acts in the opposite way: When both effects are taken into account in the charge density, the net result is a bubble weakening in ^{34}Si. In the case of the stable nucleus ^{36}S, the experimental charge distribution is available [29] and is reported on Fig. 2 as a set of black squares. The agreement with the SM profile is satisfactory.

TABLE II. Same as Table I for proton orbits in ^{36}S and ^{34}Si. Experimental occupancies obtained in Ref. [28] for ^{36}S and $S^{\rm Exp}$(^{36}S) are also reported.

Orbital	S(^{36}S)	S'(^{36}S)	$S^{\rm Exp}$(^{36}S)	S(^{34}Si)	S'(^{34}Si)
$\pi 1s_{1/2}$	2.00	1.84		2.00	1.82
$\pi 1p_{3/2}$	4.00	3.80		4.00	3.87
$\pi 1p_{1/2}$	2.00	1.90		2.00	1.94
$\pi 1d_{5/2}$	5.85	6.19	6.0(12)	5.76	6.11
$\pi 2s_{1/2}$	1.88	1.99	1.63(32)	0.08	0.09
$\pi 1d_{3/2}$	0.27	0.29	0.31(6)	0.16	0.17

It is interesting to note that the proton density depletion between the $N = 20$ isotones ^{34}Si and ^{36}S is stronger than the one reported for the $N = 16$ isotones ^{30}Si and ^{32}S derived from Ref. [30]. As seen on Fig. 4 of Ref. [30], the measured charge density for ^{30}Si does not present a significant dip at the interior of the nucleus and looks similar to that of ^{32}S. This feature comes from the modest change in occupancy of the $\pi 2s_{1/2}$ between ^{32}S(1.35) and ^{30}Si(0.65), which is ascribed to the large nuclear correlations existing in the $N = 16$ isotones. These experimental occupation numbers are in excellent agreement with the presently calculated ones, reinforcing the reliability of the SM description to model the nuclei of interest.

The reduction of proton correlations between the $N = 16$ and $N = 20$ isotones can be ascribed to the increase of the $Z = 14$ shell gap formed between the proton $d_{5/2}$ and $s_{1/2}$ orbits. While growing in size, excitations across it are progressively hampered. This results in calculated occupancies of the $\pi 2s_{1/2}$ orbit of 0.65 in ^{30}Si$_{16}$ and 0.09 in ^{34}Si$_{20}$. The driving mechanism to increase the $Z = 14$ gap is likely the strongly attractive $\pi d_{5/2}$-$\nu d_{3/2}$ proton-neutron interaction. Adding four neutrons from $N = 16$ to $N = 20$ into the $\nu d_{3/2}$ orbit strongly binds the $\pi d_{5/2}$ orbit in ^{34}Si, thus increasing the size of the $Z = 14$ shell gap.

To conclude this section, using SM calculations we have determined occupation numbers of the proton and neutron $2s_{1/2}$ shells in the (^{36}S, ^{34}Si) and (^{24}O, ^{22}O) nuclei, respectively. From these values, proton or neutron density distributions have been derived using Woods-Saxon wave functions. The large depletion of the $2s_{1/2}$ orbit gives rise to a central

density depletion and the appearance of bubble phenomena. We stress the good agreement between experimental and calculated occupation numbers for the known nuclei ^{36}S, ^{32}S, and ^{30}Si. This gives us confidence in the results obtained for the other nuclei under study. Even though the present method to derive density distributions is approximate, a reasonable agreement is found with experimental results for ^{36}S. The density profiles will be examined in the following section within a self-consistent microscopic treatment.

III. MEAN-FIELD CALCULATIONS

Self-consistent mean-field approaches enable us to determine microscopically the density distributions of nuclei. We solve the self-consistent mean-field equations directly in coordinate space. As in the previous section, we consider neutron densities for ^{22}O and proton densities for ^{34}Si. These densities should be corrected for CM effects inherent to the mean-field procedure. Since we calculate the point proton and neutron densities directly in coordinate space, we can use the Campi and Sprung procedure (see Eqs. (3.1) and (3.2) of Ref. [31]) to obtain the CM-corrected charge density of ^{34}Si, the finite proton size being treated by a Gaussian form factor as in Ref. [31]. The Fourier transform of the CM-corrected charge densities could eventually be compared with the form factors measured by electron scattering (not available so far), but accurate predictions for this kind of comparison are beyond the scope of this article. For this reason, we keep using the Gaussian finite-size form factor of Ref. [31] rather than adopting more sophisticated form factors. To obtain the radial profiles of the CM-corrected neutron densities in ^{22}O we should transform to k-space the mean-field point neutron densities, correct them with the proper CM factor, and transform back to r-space. However, the strongly model dependent results that we have obtained for ^{22}O with our mean-field treatments indicate that further refinements of the mean-field neutron densities will not help us to reach a conclusion on the issue of a possible neutron bubble in this nucleus.

For the calculation of nucleon occupation factors, pairing correlations have to be eventually taken into account. As a first step before describing the density distributions, we discuss whether pairing correlations are expected to play some role in the development of proton and neutron bubbles in ^{34}Si and ^{22}O nuclei, respectively.

A. Pairing effects

As already alluded to in Sec. I, ^{22}O is expected to behave almost as a doubly-magic nucleus, being that the $N = 14$ subshell closure has been experimentally determined. However, as shown in the previous section, SM calculations predict an 18% occupancy of the $2s$ neutron state, suggesting that pairing correlations are likely to have some effect on this nucleus. Pairing correlations will be then included and their effect on the neutron density profile of ^{22}O will be shown in the following for both the nonrelativistic and the relativistic mean-field cases.

Let us now consider the case of ^{34}Si. As an illustration, we discuss the role of pairing in the nonrelativistic case. Pairing correlations can be modeled in the Skyrme-Hartree-Fock-Bogoliubov (Skyrme-HFB) framework by adopting the following zero-range density-dependent pairing interaction:

$$V_{\text{pair}} = V_0 \left[1 - \eta \left(\frac{\rho(r)}{\rho_0} \right)^{\alpha} \right] \delta(\mathbf{r_1} - \mathbf{r_2}), \tag{2}$$

with $\eta = 0.5$ (mixed surface-volume interaction), $\alpha = 1$, and $\rho_0 = 0.16$ fm^{-3}. In the particle-hole channel, we employ the SLy4 Skyrme parametrization, which is well suited to describe neutron-rich nuclei. We fix the parameter V_0 in Eq. (2) to reproduce the two-proton separation energy in ^{34}Si. Note that the two-proton separation energy is defined as

$$S_{2p} = E(N, Z) - E(N, Z-2), \tag{3}$$

where $E(N, Z)$ is the total binding energy of the (N, Z) nucleus. It should be noted that the experimental value of $S_{2p} = 33.74$ MeV is already reasonably well reproduced without pairing: The HF value is equal to 35.19 MeV. Moreover the HFB calculations—which include the pairing interaction—yield negligible corrections, as $Z = 14$ is predicted by the HFB approach to be a robust subshell closure in agreement with the shell-model spectroscopic factors (see Table II where the SM occupation of the s state is only 4.5%). Our conclusion is that we can safely perform the analysis of this nucleus by neglecting pairing since the associated correlations are expected to be practically zero.

B. Nonrelativistic mean-field approach

Figure 3 displays neutron density profiles in ^{22}O (full line) and ^{24}O (dashed line) calculated self-consistently within the SLy4-HF approach. The depletion of the central density in ^{22}O relative to ^{24}O is clearly visible. However, the bubble profile is not obvious: Since the central neutron density in ^{24}O is strongly enhanced, the depletion in ^{22}O does not lead to the development of a significant central hole. The central depletion fraction F is ∼13%, much weaker than the SM result. As one switches on pairing and chooses the same parameters as in Ref. [32] for the pairing interaction, the central hole is seen to be partially washed out (dotted line in Fig. 3; $F = 3.4\%$).

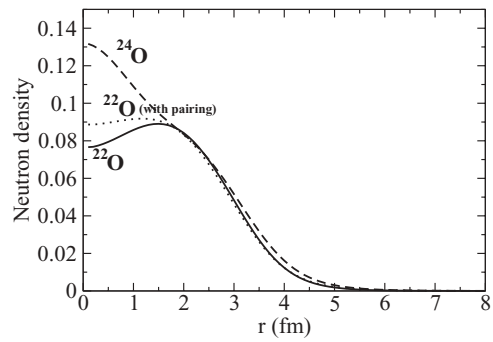

FIG. 3. HF neutron densities (in units of fm^{-3}) of ^{22}O (full line) and ^{24}O (dashed line) calculated with the Skyrme interaction SLy4. The dotted line represents the SLy4-HFB neutron density of ^{22}O.

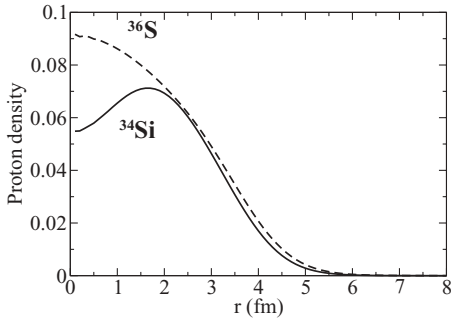

FIG. 4. HF charge densities (in units of fm^{-3}) of ^{36}S (dashed line) and ^{34}Si (solid line) calculated with the Skyrme interaction SLy4.

Note that the density profile of ^{24}O remains unchanged when pairing is switched on.

The SLy4-HF charge density profiles calculated in ^{34}Si and ^{36}S (where the s state is fully occupied) are shown in Fig. 4. One observes that the bubble is more prominent in this case than in ^{22}O. The depletion fraction F is ∼23% (38% for the proton density without CM and proton finite-size corrections). The confidence in this result is enhanced by the good agreement between the predicted density profile for ^{36}S and the experimental one shown in Fig. 2. We should mention that pairing is expected to modify the density profile of ^{36}S. By comparing the HF proton point density in ^{34}Si ($F = 38\%$) with the HF neutron density in ^{22}O ($F = 13\%$), one observes that the central value in ^{34}Si is much lower than in ^{22}O. The contribution to the central value of the density is entirely due to the first s wave function (i.e., the $1s$). The difference between the two central values may be related to the presence of a neutron excess at the surface of ^{34}Si. The effect of this neutron skin on the proton $1s_{1/2}$ wave function is to attract and push it toward the surface, thereby lowering its value at the center. This effect is obviously absent for the neutron $1s$ wave function in ^{22}O because the proton density in this nucleus is well concentrated in the interior. This can be observed in Fig. 5 where the neutron (proton) $1s$ contribution to the HF density is plotted for ^{22}O (^{34}Si).

C. Relativistic mean-field approach

As in the previous section, calculations are performed for the two oxygen isotopes ^{22}O and ^{24}O as well as for the two $N =$

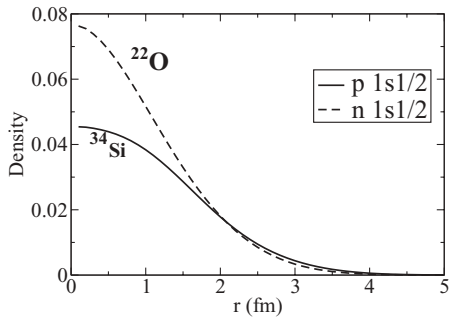

FIG. 5. Neutron (proton) $1s$ contributions to the density (in units of fm^{-3}) for ^{22}O (^{34}Si).

TABLE III. Binding energy per nucleon, charge radii, and neutron skin thickness for ^{34}Si (upper block) and ^{36}S (lower block) as predicted by the two RMF models used in this work. When available, experimental data are provided for comparison.

Model	B/A (MeV)	$R_{\rm ch}$ (fm)	$R_n - R_p$ (fm)
NL3	8.36	3.13	0.25
FSUGold	8.28	3.13	0.21
Experiment	8.34	–	–
NL3	8.50	3.26	0.12
FSUGold	8.42	3.26	0.09
Experiment	8.58	3.28	–

20 isotones ^{34}Si and ^{36}S, but now using an RMF approach. Pairing effects are evaluated within the RHB model. In one particular realization of the relativistic formalism the dynamics of the system is dictated by an interacting Lagrangian density of the following form:

$$\begin{aligned}\mathscr{L}_{\rm int} = \bar{\psi}\left[g_{\rm s}\phi - \left(g_{\rm v}V_\mu + \frac{g_\rho}{2}\tau\cdot\mathbf{b}_\mu + \frac{e}{2}(1+\tau_3)A_\mu\right)\gamma^\mu\right]\psi \\ - \frac{\kappa}{3!}(g_{\rm s}\phi)^3 - \frac{\lambda}{4!}(g_{\rm s}\phi)^4 + \frac{\zeta}{4!}\left(g_{\rm v}^2V_\mu V^\mu\right)^2 \\ + \Lambda_{\rm v}\left(g_\rho^2\,\mathbf{b}_\mu\cdot\mathbf{b}^\mu\right)\left(g_{\rm v}^2V_\mu V^\mu\right),\end{aligned} \tag{4}$$

where ψ represents an isodoublet nucleon field interacting via the exchange of two isoscalar mesons—a scalar (ϕ) and a vector (V^μ), one isovector meson (b^μ), and the photon (A^μ) [33,34]. In addition to meson-nucleon interactions, the Lagrangian density is supplemented by nonlinear meson interactions with coupling constants denoted by κ, λ, ζ, and $\Lambda_{\rm v}$ that are responsible for a softening of the nuclear-matter equation of state, both for symmetric and pure-neutron matter. For the RMF case we consider two parametrizations: the very successful NL3 parameter set [35,36] and a more recent set known as FSUGold [37]. The main difference between these two models lies in the prediction of the density dependence of the symmetry energy. This difference manifests itself in significantly larger neutron skins for NL3 than for FSUGold [37]. Neutron skins for the two isotones of interest in the present work, alongside other ground-state properties, have been listed in Table III for ^{34}Si and ^{36}S.

RMF neutron densities for the two neutron-rich isotopes ^{22}O and ^{24}O are displayed in Fig. 6. Whereas the RMF results show a mild model dependence, differences between the relativistic and nonrelativistic models are significant. Indeed, in contrast to the nonrelativistic case, the relativistic results display no enhancement of the central neutron density in ^{24}O. Moreover, the removal of both $2s_{1/2}$ neutrons from ^{24}O yields a strong depletion of the interior neutron density in ^{22}O. As a result, central depletion fractions of $F = 34\%$ $F = 28\%$ are predicted for ^{22}O by the FSUGold and NL3 models, respectively. These values are significantly larger than the 13% depletion fraction obtained with the SLy4-HF parametrization.

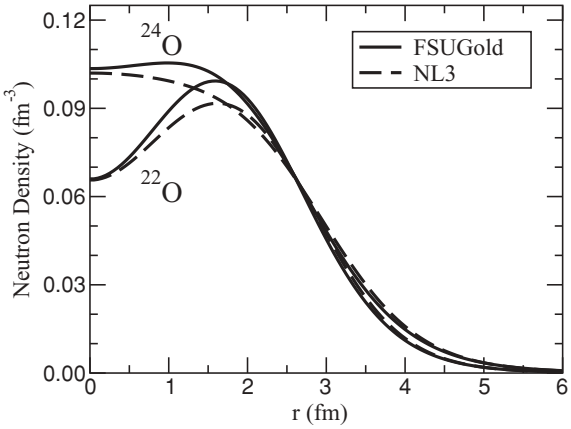

FIG. 6. RMF neutron densities of ^{22}O and ^{24}O calculated with the two RMF models described in the text.

In the case of ^{34}Si and ^{36}S one observes, now in agreement with the nonrelativistic results, how the charge density of ^{34}Si is significantly depleted in the nuclear interior and how the proton bubble disappears as soon as the $2s_{1/2}$ proton orbital is filled in ^{36}S (see Fig. 7). This behavior results in central depletion factors for ^{34}Si of $F = 29\%$ and $F = 25\%$ for the FSUGold and NL3 parameter sets, respectively. For the proton densities of ^{34}Si the values of F are 42% and 37% for FSUGold and NL3, respectively.

Let us quantify now the effects of pairing correlations within the RHB model. A medium dependence for a relativistic mean-field interaction can either be introduced by including nonlinear meson self-interaction terms in the Lagrangian, as in the case of NL3 and FSUGold, or by assuming an explicit density dependence for the meson-nucleon couplings. This is the case of the DD-ME2 model [38] that we adopt to perform RHB calculations. The couplings of the σ meson and ω meson to the nucleon are assumed to be of the form

$$g_i(\rho) = g_i(\rho_{\rm sat}) f_i(x) \quad \text{for} \quad i = \sigma, \omega, \tag{5}$$

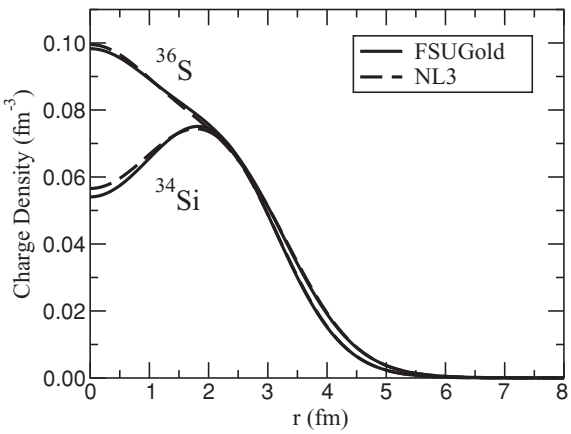

FIG. 7. RMF charge densities of ^{36}S and ^{34}Si calculated with the two RMF models described in the text.

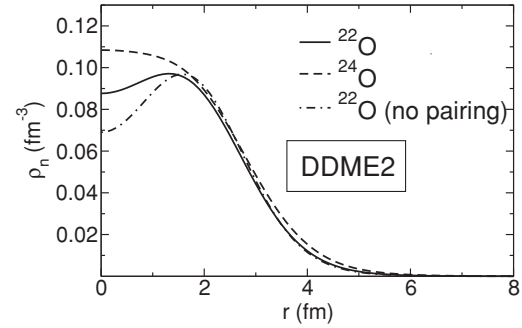

FIG. 8. Neutron density profiles of ^{22}O and ^{24}O calculated in the RHB model with the density-dependent interaction DD-ME2 and Gogny pairing.

where

$$f_i(x) = a_i \frac{1 + b_i(x + d_i)^2}{1 + c_i(x + d_i)^2} \tag{6}$$

is a function of $x = \rho/\rho_{\rm sat}$, and $\rho_{\rm sat}$ denotes the nucleon density at saturation in symmetric nuclear matter. Constraints at nuclear matter saturation density and at zero density are used to reduce the number of independent parameters in Eq. (6) to three. Three additional parameters in the isoscalar channel are $g_\sigma(\rho_{\rm sat})$, $g_\omega(\rho_{\rm sat})$, and m_σ—the mass of the phenomenological σ meson. For the ρ meson coupling the functional form of the density dependence is suggested by Dirac-Brueckner calculations of asymmetric nuclear matter:

$$g_\rho(\rho) = g_\rho(\rho_{\rm sat}) \exp[-a_\rho(x - 1)], \tag{7}$$

and the isovector channel is parametrized by $g_\rho(\rho_{\rm sat})$ and a_ρ. Bare values are used for the masses of the ω and ρ mesons: $m_\omega = 783$ MeV and $m_\rho = 763$ MeV. DD-ME2 is determined by eight independent parameters, adjusted to the properties of symmetric and asymmetric nuclear matter, binding energies, charge radii, and neutron radii of spherical nuclei [38]. The interaction has been tested in the calculation of ground-state properties of a large set of spherical and deformed nuclei. When used in the relativistic RPA, DD-ME2 reproduces with high accuracy data on isoscalar and isovector collective excitations [38].

In Figs. 8 and 9 we display, respectively, the neutron and charge density profiles for ^{22,24}O (^{34}Si and ^{36}S) calculated in

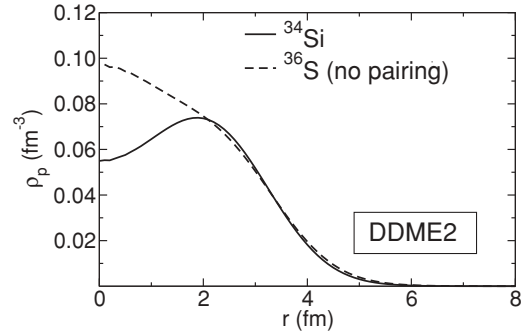

FIG. 9. Charge densities of ^{36}S and ^{34}Si calculated in the RHB model with the DD-ME2 interaction plus Gogny D1S pairing. The charge density of ^{36}S has been calculated by neglecting pairing.

TABLE IV. Central fraction of depletion F for neutron densities in ^{22}O (first line) and proton and charge densities in ^{34}Si (second and third lines, respectively).

Nucleus	SM	SLy4 HF	SLy4 HFB	NL3 RMF	FSUGold RMF	DDME2 RMF	DDME2 RHB
^{22}O	24%	13%	3.4%	28%	34%	29%	10%
^{34}Si	41%	38%	38%	37%	42%	36%	36%
^{34}Si (ch.)	28%	23%	23%	25%	29%	25%	25%

the RHB model [39] with the DD-ME2 effective interaction in the particle-hole channel, and with the Gogny interaction [40] in the pairing channel,

$$V^{pp}(1,2) = \sum_{i=1,2} e^{-[(\mathbf{r}_1-\mathbf{r}_2)/\mu_i]^2} \times (W_i + B_i P^\sigma - H_i P^\tau - M_i P^\sigma P^\tau), \quad (8)$$

with the set D1S [41] for the parameters μ_i, W_i, B_i, H_i, and M_i ($i = 1, 2$).

For ^{24}O and ^{34}Si the RHB calculation with the DD-ME2 interaction predicts neutron and charge density profiles similar to those calculated with NL3 and FSUGold. Because of the large gaps between $\nu s_{1/2}$ and $\nu d_{3/2}$ in ^{24}O, and between $\pi d_{5/2}$ and $\pi s_{1/2}$ in ^{34}Si, we find a pairing collapse in these nuclei, in agreement with nonrelativistic predictions. However, the inclusion of pairing correlations has a pronounced effect on the neutron density profile in ^{22}O. When pairing is set to zero (dash-dot curve in Fig. 8) the $\nu s_{1/2}$ orbital is empty in ^{22}O. The resulting DD-ME2 density profile is again very similar to that calculated with the two other RMF interactions. However, the pairing interaction in the RHB model calculation modifies the occupancy of the two $2s_{1/2}$ orbitals, thus reducing the pronounced bubble in the neutron density of ^{22}O. For an easier and coherent comparison between Figs. 4 and 9, the charge density of ^{36}S shown in Fig. 9 has been calculated by neglecting pairing.

In the DD-ME2 model the F values are found equal to 29%, 10%, and 25% for ^{22}O (without pairing), ^{22}O (with pairing), and charge density of ^{34}Si (giving the same result with and without pairing), respectively. For the proton density of ^{34}Si $F = 36\%$.

IV. SUMMARY AND CONCLUSIONS

The occurrence of proton and neutron bubbles in ^{34}Si and ^{22}O, respectively, has been investigated using three different theoretical approaches: (i) the shell model, (ii) the Skyrme mean-field model, and (iii) the relativistic mean-field model. This occurrence can be quantified by the values of the depletion fraction F, which we have evaluated in these different approaches and which are summarized in Table IV.

For the ^{22}O nucleus the CM correction has been performed only in the SM framework. The strongly model dependent results that we have obtained for this nucleus with our mean-field treatments indicate that further refinements of the mean-field neutron densities will not help us to reach a conclusion on the issue of a possible neutron bubble. To compare in a coherent way all the values of F for ^{22}O in Table IV, the SM values without CM correction have been used. Indeed, a very significant model dependence has been found for this nucleus. Moreover, in both nonrelativistic and relativistic cases, pairing correlations have been shown to weaken the bubble phenomenon. It would be worth having experimental confirmation of this prediction. In contrast, for ^{34}Si an overall agreement exists: A central depletion fraction of $\sim$40% is predicted by all the models for the proton densities. In the last line of Table IV, the values of F for the charge density are shown ($F \sim 25\%$–30%).

The strong model dependence for ^{22}O and the overall agreement for ^{34}Si are easy to explain. For both nuclei the single-particle spectra are sensibly model dependent. However, the gap $N = 14$ is predicted by all the models to be much smaller than the gap $Z = 14$. The very large gap $Z = 14$ prevents pairing and other correlations from being active in ^{34}Si, providing thus density profiles that are not sensible to the differences of the models. In contrast, for ^{22}O, pairing plays some role and, consequently, the density profiles show a dependence on the model (based on single-particle spectra and intensity of pairing interaction). This reinforces the conclusion that ^{34}Si is indeed a good candidate for a bubble density profile. The measurement of the charge density in ^{34}Si could be undertaken, for instance, by electron scattering in an exotic beam collider, such as EXL in FAIR and RIBF in Riken. The bubble impact on the momentum distribution in these experiment has been investigated in Ref. [8]. The fraction F for the charge densities is equal to $\sim$25%–30%. The effect is reduced with respect to what is found for the proton densities, but it is still important and could be observed experimentally. The study of ^{34}Si, either by high-energy proton scattering (to focus on the matter distribution) or by direct reactions (to determine whether the occupancy of the $2s_{1/2}$ proton orbit has dropped to nearly zero, thus confirming the SM predictions shown in Sec. II.), is already feasible [8].

ACKNOWLEDGMENTS

The authors thank J. F. Berger, A. E. L. Dieperink, F. Nowacki, A. Poves, and K. Yoshida for valuable discussions. The research of J.P. is supported in part by the United States DOE Grant No. DE-FD05-92ER40750.

[1] H. A. Wilson, Phys. Rev. **69**, 538 (1946).
[2] X. Campi and D. W. L. Sprung, Phys. Lett. **B46**, 291 (1973).
[3] M. Bender, K. Rutz, P.-G. Reinhard, J. A. Maruhn, and W. Greiner, Phys. Rev. C **60**, 034304 (1999).
[4] J. Dechargé, J.-F. Berger, M. Girod, and K. Dietrich, Nucl. Phys. **A716**, 55 (2003).
[5] J. M. Cavedon *et al.*, Phys. Rev. Lett. **49**, 978 (1982).
[6] V. R. Pandharipande, I. Sick, and P. K. A. deWitt Huberts, Rev. Mod. Phys. **69**, 981 (1997).
[7] B. G. Todd-Rutel, J. Piekarewicz, and P. D. Cottle, Phys. Rev. C **69**, 021301(R) (2004).
[8] E. Khan, M. Grasso, J. Margueron, and N. Van Giai, Nucl. Phys. **A800**, 37 (2008).
[9] L. Gaudefroy *et al.*, Phys. Rev. Lett. **99**, 099202 (2007).
[10] A. Gade *et al.*, Phys. Rev. C **74**, 034322 (2006).
[11] M. Grasso, Z. Y. Ma, E. Khan, J. Margueron, and N. Van Giai, Phys. Rev. C **76**, 044319 (2007).
[12] O. Sorlin and M. G. Porquet, Prog. Part. Nucl. Phys. **61**, 602 (2008).
[13] K. Yoshida (private communication).
[14] S. Hilaire and M. Girod, http://www-phynu.cea.fr/science_en_ligne/carte_potentiels_microscopiques/carte_potentiel_nucleaire.htm (2006).
[15] S. Raman, C. W. Nestor Jr., and P. Tikkanen, At. Data Nucl. Data Tables **78**, 1 (2001).
[16] B. Bastin *et al.*, Phys. Rev. Lett. **99**, 022503 (2007).
[17] M. Stanoiu *et al.*, Phys. Rev. C **69**, 034312 (2004).
[18] A. Schiller *et al.*, Phys. Rev. Lett. **99**, 112501 (2007).
[19] Z. Elekes *et al.*, Phys. Rev. Lett. **98**, 102502 (2007).
[20] P. G. Thirolf *et al.*, Phys. Lett. **B485**, 16 (2000).
[21] E. Becheva *et al.*, Phys. Rev. Lett. **96**, 012501 (2006).
[22] C. R. Hoffman *et al.*, Phys. Rev. Lett. **100**, 152502 (2008).
[23] E. Caurier, ANTOINE code, IReS, Strasbourg, 1989–2002.
[24] E. Caurier and F. Nowacki, Acta Phys. Pol. B **30**, 705 (1999).
[25] B. A. Brown and B. H. Wildenthal, Annu. Rev. Nucl. Part. Sci. **38**, 29 (1988).
[26] A. E. L. Dieperink and T. de Forest Jr., Phys. Rev. C **10**, 543 (1974).
[27] A. Bohr and B. R. Mottelson, *Nuclear Structure* (Benjamin, New York, 1975), Vol. I.
[28] S. Khan *et al.*, Phys. Lett. **B156**, 155 (1985).
[29] D. Rychel *et al.*, Phys. Lett. **B130**, 5 (1983).
[30] J. Wesseling *et al.*, Phys. Rev. C **55**, 2773 (1997).
[31] X. Campi and D. W. L. Sprung, Nucl. Phys. **A194**, 401 (1972).
[32] E. Khan, N. Sandulescu, M. Grasso, and N. Van Giai, Phys. Rev. C **66**, 024309 (2002).
[33] B. D. Serot and J. D. Walecka, Adv. Nucl. Phys. **16**, 1 (1986).
[34] B. D. Serot and J. D. Walecka, Int. J. Mod. Phys. E **6**, 515 (1997).
[35] G. A. Lalazissis, J. Konig, and P. Ring, Phys. Rev. C **55**, 540 (1997).
[36] G. A. Lalazissis, S. Raman, and P. Ring, At. Data Nucl. Data Tables **71**, 1 (1999).
[37] B. G. Todd-Rutel and J. Piekarewicz, Phys. Rev. Lett. **95**, 122501 (2005).
[38] G. A. Lalazissis, T. Nikšić, D. Vretenar, and P. Ring, Phys. Rev. C **71**, 024312 (2005).
[39] D. Vretenar, A. V. Afanasjev, G. A. Lalazissis, and P. Ring, Phys. Rep. **409**, 101 (2005).
[40] J. F. Berger, M. Girod, and D. Gogny, Nucl. Phys. **A428**, 23 (1984).
[41] J. F. Berger, M. Girod, and D. Gogny, Comput. Phys. Commun. **63**, 365 (1991).